Frequency Domain Analysis of the Distribution Function by Small Signal Solution of the Boltzmann and Poisson Equations

C.-K Lin, N. Goldsman, Z. Han, I. Mayergoyz, S. Yu*, M. Stettler* and S. Singh*
Dept. of Electrical Engineering, University of Maryland, College Park, MD 20742, USA
*Intel Corporation, Hillsboro, OR 97124

Abstract A method for solving the Boltzmann-Poisson system in the frequency domain has been developed. It is achieved by applying small signal analysis to the Spherical Harmonic expansion method of solving the Boltzmann Equation. By solving this model in the frequency domain, we can investigate the frequency response of entire momentum distribution function. A 0.05 μm base BJT simulation in frequency domain gives the results of the small signal distribution function response over the entire device in 4 minutes CPU time on an Alpha workstation.

I. Introduction

As IC operating speeds increase into the gigahertz range, understanding the frequency response of devices becomes increasingly important. To meet this challenge, we have developed a method for solving the Boltzmann transport equation and Poisson equation self-consistently in the frequency domain. Previous investigators have solved the Drift-Diffusion (DD) model in the frequency domain which gave the frequency dependence of the carrier concentrations and electrostatic potential within the limits of the DD model[1,2]. By solving the Boltzmann-Poisson model in the frequency domain, we not only account for the effects of velocity overshoot on ensemble averages, but determine the frequency response of the entire momentum distribution function. By ascertaining how each part of the distribution function responds to frequency of operation, insight can be gained into the frequency-dependent transport of electrons in phase-space. With this added information, we open the door to using this knowledge for improved high-speed device design.

2. Small Signal Model

To investigate the frequency response of the distribution function for small sinusoidal voltage inputs, we use a mathematical/physical device model which consists of the Poisson Equation, the time-dependent Boltzmann Transport Equation (BTE) for electrons, and the time-dependent Current Continuity Equation for holes.

$$F_\phi = \nabla^2_{\vec{r}}\phi(\vec{r},t) - \frac{q}{\epsilon_s}\left[\int f(\vec{k},\vec{r},t)d\vec{k} - p(\vec{r},t) + D(\vec{r})\right] \tag{1}$$

$$F_f = -\frac{\partial f(\vec{r},\vec{k},t)}{\partial t} + \frac{-\nabla_k \varepsilon}{\hbar}\cdot\nabla_{\vec{r}} f(\vec{k},\vec{r},t) - \frac{e}{\hbar}\nabla_{\vec{r}}\phi(\vec{r},t)\cdot\nabla_k f(\vec{k},\vec{r},t) + \left[\frac{\partial f(\vec{k},\vec{r},t)}{\partial t}\right]_c \tag{2}$$

$$F_p = -\frac{\partial p(\vec{r},t)}{\partial t} + \nabla_{\vec{r}}\cdot[\mu_p p(\vec{r},t)\nabla_{\vec{r}}\phi(\vec{r},t) + \mu_p V_t \nabla_{\vec{r}} p(\vec{r},t)] - R(\phi,n,p) \tag{3}$$

$f(\vec{r},\vec{k},t)$ is the electron distribution function; $\phi(\vec{r},t)$ is the potential; $p(\vec{r},t)$ is the hole concentration; $D(\vec{r})$ is the net doping concentration; $R(n,p)$ is the net hole recombination rate; $V_t = K_B T/q$ is the thermal voltage; ϵ_s is the dielectric constant of silicon.

In this work we focus on small signal operation where we determine a DC operating point, and then perturb it by adding a small AC component.

$$\phi = \phi_0(\vec{r}) + \tilde{\phi}(\vec{r},\omega)e^{j\omega t}, \quad f = f_0(\vec{r},\vec{k}) + \tilde{f}(\vec{r},\vec{k},\omega)e^{j\omega t} \quad p = p_0(\vec{r}) + \tilde{p}(\vec{r},\omega)e^{j\omega t} \tag{4}$$

where suffix "o" denotes self-consistent DC steady-state solution; "$\sim$" denotes the complex AC small signal component; ω is the frequency. We then can linearize the Eqns. (1,2,3) about the DC operating point with the Taylor first order expansion:

$$F_\phi(\phi,f,p) = F_\phi(\phi_0,f_0,p_0) + \left.\frac{\partial F_\phi(\phi,f,p)}{\partial\phi}\right|_{dc}\cdot\tilde{\phi}e^{j\omega t} + \left.\frac{\partial F_\phi(\phi,f,p)}{\partial f}\right|_{dc}\cdot\tilde{f}e^{j\omega t} + \left.\frac{\partial F_\phi(\phi,f,p)}{\partial p}\right|_{dc}\cdot\tilde{p}e^{j\omega t} = 0 \tag{5}$$

$$F_f(\phi,f,p) = F_f(\phi_0,f_0,p_0) - j\omega\tilde{f}e^{j\omega t} + \left.\frac{\partial F_f(\phi,f,p)}{\partial\phi}\right|_{dc}\cdot\tilde{\phi}e^{j\omega t} + \left.\frac{\partial F_f(\phi,f,p)}{\partial f}\right|_{dc}\cdot\tilde{f}e^{j\omega t} + \left.\frac{\partial F_f(\phi,f,p)}{\partial p}\right|_{dc}\cdot\tilde{p}e^{j\omega t} = 0 \tag{6}$$

$$F_p(\phi,f,p) = F_p(\phi_0,f_0,p_0) - j\omega\tilde{p}e^{j\omega t} + \left.\frac{\partial F_p(\phi,f,p)}{\partial \phi}\right|_{dc}\cdot\tilde{\phi}e^{j\omega t} + \left.\frac{\partial F_p(\phi,f,p)}{\partial f}\right|_{dc}\cdot\tilde{f}e^{j\omega t} + \left.\frac{\partial F_p(\phi,f,p)}{\partial p}\right|_{dc}\cdot\tilde{p}e^{j\omega t} = 0 \tag{7}$$

The objective at this point is to obtain the small signal coefficients $\tilde{\phi}(\vec{r},\omega)$, $\tilde{f}(\vec{r},\vec{k},\omega)$ and $\tilde{p}(\vec{r},\omega)$

3. Solution

We obtain the small signal coefficients numerically. For equations (1) and (3) we follow fairly typical methodologies where we discretize first, and then determine the small signal coefficients from the discretized equations[1]. The BTE, however, is considerably more complicated, and it will thus be our primary focus. Before discretizing the BTE, we transform it into a tractable form by extending the SH formulation[3], to the frequency domain. To achieve this we write the DC and AC parts of the distribution function in terms of spherical harmonics:

$$f(\vec{r},\vec{k},t) = \sum_{l,m}\left[f_{0,l,m}(\vec{r},k) + \tilde{f}_{l,m}(\vec{r},k,t)\right]Y_l^m \tag{8}$$

Then we substitute this expression into Eq(2). Taking advantage of recurrence and orthogonality between Spherical Harmonic basis functions, a system of equations for the expansion coefficients can be obtained. After truncating the high order terms, we build upon the DC formulation[3], and discretize the BTE by a Scharfetter-Gummel method to obtain the following:

$$\begin{aligned} F_{fi} \;=\; & -j\omega\tilde{f}_i e^{j\omega t} + \alpha_{i+1/2,m}(f_{i+1,m} - f_{i,m}) - \alpha_{i-1/2,m}(f_{i,m} - f_{i-1,m}) \\ & + \beta_{i,m-ln}(f_{i,m-ln} - e^{\hbar\omega_n/K_0T} f_{i,m}) + \beta_{i,m+ln}(e^{\hbar\omega_n/K_0T} f_{i,m+ln} - f_{i,m}) \end{aligned} \tag{9}$$

where $f_{i,m} = f_{0,i,m} + \tilde{f}_{i,m}e^{j\omega t}$; i=real space domain mesh index; m=energy domain mesh index; $l_n = \frac{\hbar\omega}{\triangle H}$; $\triangle H = \triangle(\varepsilon - q\phi)$=energy mesh (uniform); h_i=real space mesh (non-uniform);

$\alpha_{i+1/2,m} = \frac{S_{i+1,m}-S_{i,m}}{ln(S_{i+1,m})-ln(Si,m)}\frac{2}{h_i(h_i+h_{i+1})}$ $\qquad$ $\alpha_{i-1/2,m} = \frac{S_{i-1,m}-S_{i,m}}{ln(S_{i-1,m})-ln(Si,m)}\frac{2}{h_i(h_i+h_{i+1})}$;

$\beta_{i,m-ln} = \frac{3(\varrho-1)D_n^2 m^{*2}}{2\pi\hbar^3\rho\omega_n}\frac{\sqrt{\gamma_{i,m}}\gamma'_{i,m}}{e^{\hbar\omega_n/K_0T}-1}\sqrt{\gamma_{i,m-ln}}\gamma'_{i,m-ln}$ $\qquad$ $\beta_{i,m+ln} = \frac{3(\varrho-1)D_n^2 m^{*2}}{2\pi\hbar^3\rho\omega_n}\frac{\sqrt{\gamma_{i,m}}\gamma'_{i,m}}{e^{\hbar\omega_n/K_0T}-1}\sqrt{\gamma_{i,m+ln}}\gamma'_{i,m+ln}$;

$S_{i,m} = \gamma_{i,m}\tau_{i,m}v_{i,m}$; $\gamma = \frac{\hbar^2k^2}{2m^*}$ is the dispersion relation; $\frac{1}{\tau}$ = total scattering rate; v = electron group velocity; m^* = effective mass.

After discretizing equations (1) (2) and (3), we can begin to determine the small signal coefficients. To achieve this, we perform a first order Taylor expansion about the DC solution of the discretized equations (eqn. (9) for the BTE). To the Taylor series, we must also add the first order terms originating from the $\partial f/\partial t$ and $\partial p/\partial t$. This gives rise to the Jacobian-type matrix with additional $j\omega$ terms along the diagonal, as shown in Fig(1a). The $\bar{R}$ vector consists of zeros, except where the boundary conditions are implemented.

$$\begin{pmatrix} \left(\frac{\partial F_\phi}{\partial\phi}\right)_{N\times N} & \left(\frac{\partial F_\phi}{\partial f}\right)_{N\times NM} & \left(\frac{\partial F_\phi}{\partial p}\right)_{N\times N} \\ \left(\frac{\partial F_f}{\partial\phi}\right)_{NM\times N} & \left(\frac{\partial F_f}{\partial f} - jwI\right)_{NM\times NM} & \left(\frac{\partial F_f}{\partial p}\right)_{NM\times N} \\ \left(\frac{\partial F_p}{\partial\phi}\right)_{N\times N} & \left(\frac{\partial F_p}{\partial f}\right)_{N\times NM} & \left(\frac{\partial F_p}{\partial p} - jwI\right)_{N\times N} \end{pmatrix} \begin{pmatrix} \tilde{\phi}_N \\ \tilde{f}_{NM} \\ \tilde{p}_N \end{pmatrix} = \bar{R}$$

(a)

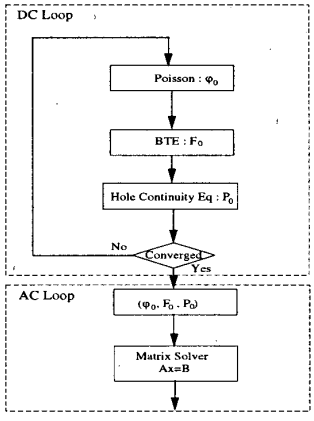

(b)

Figure 1: (a) The formation of Jocabian matrix. N and M are number of space and energy mesh respectively. (b) Simulation Flow Chart.

With the small signal equations formulated, we solve the frequency domain model according to the flow chart in Fig(1b). For one particular DC bias, we first calculate a self-consistent solution (ϕ_0, f_0, p_0). Using the resulting DC solution, the elements of the Jacobian are evaluated. The linear system can be solved by SuperLU complex number matrix solver[4] to obtain $(\tilde{\phi}, \tilde{f}, \tilde{p})$ at each particular frequency.

4. Simulation Results

We used the above model to simulate a 0.05 μm base BJT. First, V_{BE}=0.95V and V_{BC}=1V DC values are applied on two side terminals, and we obtain a self-consistent DC solution. In Fig(2) we show the doping profile, resulting electric field respectively. The DC normalized energy distribution function is shown in

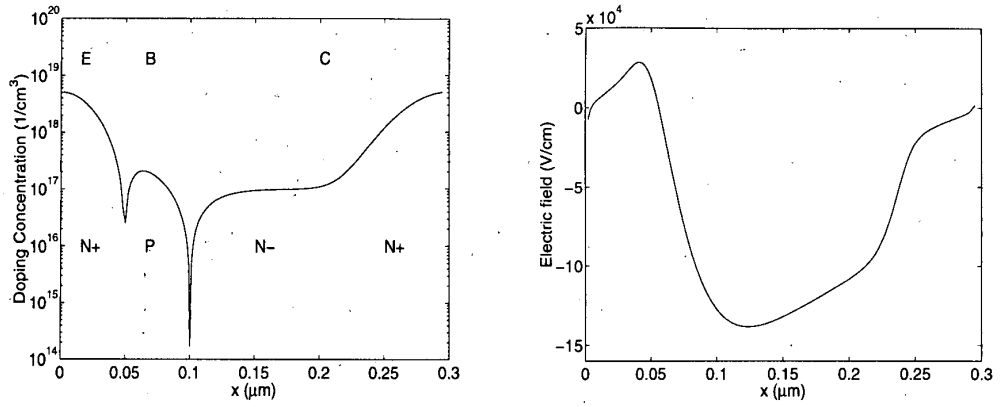

(a) (b)

Figure 2: (a) Simulated BJT Doping Profile. (b) Calculated DC Electric Field.

Fig(3a). Next, we applied a small perturbation voltage $V_{be} = 0.1V_t$ to the BJT emitter. The range of input frequencies is from 1K Hz to 10G Hz. Fig(3b) shows the normalized magnitude $|\tilde{f}| = (\sqrt{Re(\tilde{f})^2 + Im(\tilde{f})^2})$ of the AC energy distribution function over the whole device at ω = 10GHz. Fig(3b) indicates that the AC component of energy distribution function departs from the DC distribution function especially for values of high energy. Fig(4a) shows the ratio of the AC to DC distribution functions at different locations. The

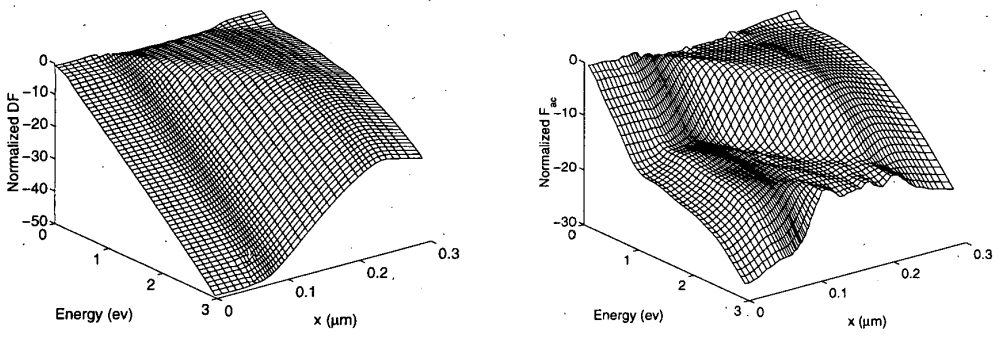

(a) (b)

Figure 3: (a) DC electron energy distribution function. (b) Magnitude of AC electron energy distribution function throughout device at 10GHz.

figure indicates that relatively speaking, the high-energy tail of the distribution function is more effected by the AC signals, and the effect decreases as the DC distribution function becomes more heated. Fig(4b) shows that the low energy electrons are in phase with the applied voltage, but the higher ones are out of

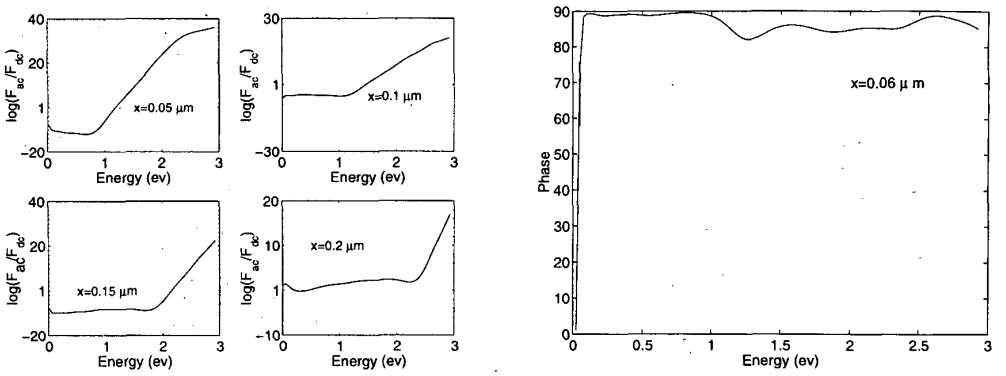

(a) (b)

Figure 4: (a)Ratio of AC to DC distribution functions at locations x=0.05μm, 0.1μm, 0.15μm, 0.2μm. (b) AC distribution function phase versus energy at x=0.06μm and 10GHz

phase. This indicates that the low and high energy electrons diffuse at different rates. This agrees with theoretical results obtained for time domain calculations which indicate that high energy electrons transport first in BJT's leading to energy overshoots[5].

The current in the device can be divided into a displacement current as well as an AC and a DC particle current, with the magnitude constant:

$$|J_{dis} + J^{dc}_{par} + J^{ac}_{par}| = |(j\omega)\epsilon_s \cdot \tilde{E}e^{j\omega t} + J_0 + \tilde{J}e^{j\omega t}| = constant \tag{10}$$

The current is determined directly by multiplying the calculated distribution function by velocity and integrating over momentum space. Fig(5) shows the current for the real and imaginary parts of $|J_{dis} + J^{ac}_{par}|$ at the frequency 10G Hz. The figure shows that the magnitudes of the particle and displacement currents sum to a constant to preserve continuity.

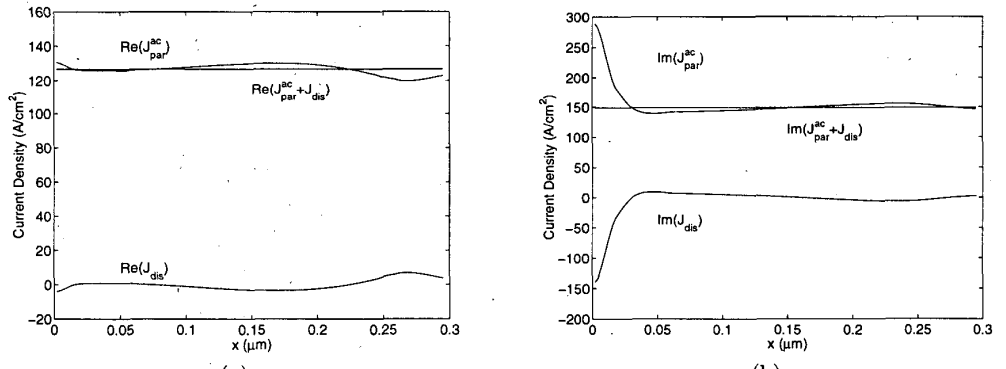

(a) (b)

Figure 5: At 10G Hz (a)Real part of $J_{dis} + J^{ac}_{par}$ vs position. (b)Imaginary part of $J_{dis} + J^{ac}_{par}$ vs position.

1. S. Laux; *IEEE Trans. on Elec. Dev.*, vol. 32, pp. 2028–2037, 1985.
2. F. M. Rotella; Z. Yu; R. Dutton; *SISPAD 97*, pp. 157–159,1997.
3. W. Liang; N. Goldsman; I. Mayergoyz; and P. Oldiges; *IEEE Trans. on Elec. Dev.*, vol. 44, pp. 257–276, 1997.
4. James W. Demmel; John R. Gilbert; Xiaoye S. Li; *SuperLU Users' Guide. http://http.cs.berkeley.edu/ xiaoye/superlu.html.*
5. C.-K Lin; N. Goldsman; Isaak D. Mayergoyz and Chien-Hwa Chang; *Journal of Applied Physics*, vol. 86, No.1, July, 1999.